Int. J. Electrochem. Sci., 13 **(2018)** 11867 – 11881, doi: 10.20964/2018.12.79

International Journal of
ELECTROCHEMICAL
SCIENCE
www.electrochemsci.org

Enhanced Dispersion of Graphene in Epoxy-Acrylic Waterborne Anticorrosion Coating: Bifunctional Ligands Linking Graphene to SiO_2

Lei Guo[1#], *Lingzhi Jing*[1#], *Yan Liu*[1], *Bingjie Zou*[1], *Sicheng Hua*[1], *Jiangpeng Zhang*[1], *Dayang Yu*[1], *Shuchuan Wang*[2], *Shirong Wang*[2], *Lidong Wang*[3,*], *Jingxia Yang*[1,2,3,*]

[1] College of Chemistry and Chemical Engineering, Shanghai University of Engineering Science, LongTeng Road 333, 201620 Shanghai, P. R. China
[2] T&H chemicals CO. LTD, Tangxi Industrial Zone, Quanzhou Luojiang District, 362011, Fujian, P.R. China
[3] School of Materials Science and Engineering, Harbin Institute of Technology, Harbin, 150001, China
[#]L. Guo and L. Jing contributed equally to this work.
[*]E-mail: yjx09tj@foxmail.com, wld@hit.edu.cn

Received: 8 September 2018 / *Accepted:* 11 October 2018 / *Published:* 5 November 2018

The dispersion of graphene was improved by using a bifunctional ligand *p*-aminobenzoic acid (PABC) to anchor graphene (Gr) to SiO_2 particles (marked as SiO_2-PABC-Gr). This can avoid the phase separation and improve the dispersion of graphene in coatings. The materials were characterized by Fourier transform infrared spectroscopy (FT-IR), scanning electron microscope (SEM), X-ray diffraction (XRD) and Raman spectra to prove the linking structure. An epoxy-acrylic (EA) resin was used as the binder, which contained COOH groups to connect with SiO_2 particles. The synthesized SiO_2-PABC-Gr (1 wt%) was dispersed in EA resin and used as anticorrosion protection composite coating of low carbon steel, and the corrosion resistance was investigated by potentiodynamic polarization curve and electrochemical impedance spectroscopy (EIS). The results indicated that graphene was successfully linked to SiO_2 by PABC, and the application in EA resin can significantly improve the anticorrosion ability of the coating, which can be attributed to the high dispersion of graphene.

Keywords: Anticorrosion; graphene dispersion; composite; epoxy-acrylic resin; waterborne coating; bifunctional ligand

1. INTRODUCTION

Waterborne resin has been widely studied and used nowadays due to the less volatile organic compounds (VOCs) release [1-4], which is beneficial to the environment and human's health. The

anticorrosive performance is very important for the waterborne resins used as metal coating. In order to enhance the anticorrosive performance, many approaches have been developed to reduce the polar channels formed by the resin chain rearrangement during the solvent evaporation, such as improving the crosslinking degree of the resin [5], incorporating inorganic barriers to block the hole (especially sheet or flake like material [6-9]) and so on. As the most famous sheet material, graphene and its derivatives have been studied widely in anticorrosion application (eg.[7-24]).

Graphene can be divided into two categories according to the defect concentration: (1) graphene sheet with few defects, produced by mechanical exfoliation [25-29], epitaxial growth on SiC [30-31] and combustion synthesis [32-35], etc. Since the concentration of the functional groups which can connect with polymer or inorganic oxide particles is low, the dispersion of graphene could be an issue; (2) graphene with lots of defects, synthesized by the reduction of graphene oxide [36-38]; this kind of graphene normally bears many functional groups, making it more easily to disperse in water and connect with resin or inorganic oxide. In order to well disperse graphene into coating, surface modification was adopted by using some silane coupling agent (eg. 3-aminopropyl triethoxysilane), to link graphene with the resin[6]. But silane coupling agents are sensitive to H_2O, and the modification processing has to be done in non-aqueous condition, which makes the application complicated in waterborne resin.

In this research, epoxy-acrylic (EA) waterborne resin was used as the binder of the anticorrosive coating for low carbon steel, which was highly crosslinking and with carboxylic acid groups to connect with oxide fillers; both hydrophobic graphene sheets with few defects and hydrophilic SiO_2 particles were used as the fillers to block the polar channels. The sheet structure of graphene has been proved that they can block pin-holes and so on in the coating films [7-24], while SiO_2 particles were a kind of common filler used in coating. However, the great difference of the hydrophilicity between the two fillers makes them difficult to be homogeneously dispersed in the coating, and the separation of SiO_2 particles and graphene sheets could happen. To solve this problem, a new linking method was developed to connect SiO_2 and graphene to produce a composite and avoid the agglomerations, by using the ligand with two functional groups (*p*-aminobenzoic acid). This approach can be carried out in both aqueous and non-aqueous conditions. The synthesized composites were characterized by Fourier transform infrared spectroscopy (FT-IR), scanning electron microscope (SEM), X-ray diffraction (XRD), Raman spectra and so on. The electrochemical measurements were used to evaluate the corrosion behaviors of low carbon steel with the prepared coating.

2. EXPERIMENTAL SECTION

Material used: Graphene were provided by T&H chemicals Co. LTD, tetraethyl orthosilicate(TEOS) polyvinylpyrrolidone(PVP) K10-K14, terephthalic acid (PCBC), ammonium hydroxide solution and 4-Aminobenzoic acid (PABC) were purchased from Energy Chemical Co. LTD. Waterborne epoxy resin was supplied by Usolf Co. LTD.

2.1 Synthesis and Modification of SiO_2 particles

Silica sphere particles of 500 nm were synthesized according to Stöber method [39-40]. 60 ml tetraethyl orthosilicate ($Si(OEt)_4$) were put into a solution containing 320 mL ethanol (EtOH) and 240 mL H_2O, and hydrolyzed and condensed by adding 200 mL ammonium hydroxide (NH_4OH). The mixture reacted at room temperature (c.a. 25 °C) for 2h. Then the white solution was centrifuged and washed by EtOH for 3 times. The obtained white precipitate was collected and dried at 60 °C in vacuum oven. The dried solids were grinded, and further used for modification.

The modification routes were sketched in Figure 1. Graphene sheets were provided by T&H chemicals CO. LTD and produced by a combustion method based on an exothermal reaction between Mg and $CaCO_3$ [33]. *p*-Aminobenzoic acid (PABC) was used as a bifunctional ligand to connect SiO_2 and graphene. In beaker A, 0.6 g SiO_2 particles were ultrasonic dispersed in 30 mL EtOH for 30 min. Then 2 mmol PABC was added and stirred for 15 min. In beaker B: 0.005 g graphene was ultrasonically dispersed in 20 mL EtOH for 30 min, and then added into beaker A. The mixture was further stirred for 15 min and then dispersed by high speed homogenizer (10000 rmp) for 10 min. The composites were centrifuged (5000 rmp) and no phase separation was observed. It's dried at 60 °C in vacuum oven and grinded afterwards. The dried solid was blue-grey color, and marked as SiO_2-PABC-Gr. In this procedure, solvent EtOH can be substituted by H_2O.

For comparison, *p*-phthalic acid (PCBC) was also used as another bifunctional ligand. The synthesis procedure was the same as the above, by using the same mole PCBC instead of PABC. There was an obvious phase separation during the centrifugation processing, as shown in Figure 1. The prepared solid was grey color and named as SiO_2-PCBC-Gr.

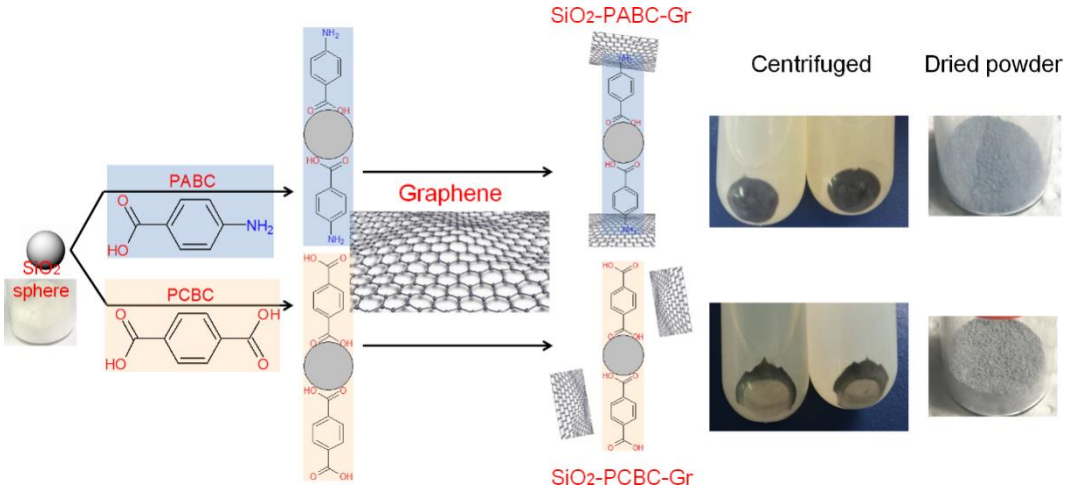

Figure 1. Modifications of SiO_2 by graphene via bifunctional ligands

2.2 Synthesis of epoxy-acrylic (EA) resin

EA resins were synthesized according to the research by M. Liu et.al, which was a two-step esterification process [5]. Here we describe the procedure briefly. In the first esterification, epoxy monomers (E20) reacted with the same mole ratio n-octanoic acid by using a certain amount of N,N-

dimethylethanolamine (DMEA) as catalyst. The mixture reacted at 105 °C for 100 min to form the epoxy-octanoic ester (EP). Poly-acrylic (PA) prepolymer was prepared though a free radical polymerization of three different acrylic monomers. The monomer mixture was formed by methacrylic acid (MAA), methymethacrylate (MMA), and n-butyl acrylate (BA), by using azoisobutyronitrile (AIBN) as initiator and n-dodecyl mercaptan (NDM) as chain transfer agent. The reaction took place at 85 °C and lasted for c.a. 90 min.

The second esterification step was the reaction between the prepared EP and PA prepolymers. Based on solid contents of the resultant solutions, the mass ratio of EP to PA was 3:7 by using a certain amount of DMEA as catalyst. The reaction condition was 105 °C for 100 min, and EA graft copolymer (EA resin, which structure was predicted according to ref [5] as shown in

Figure **2**) was prepared. The prepared EA resin was neutralized by DMEA and diluted to 40 wt.% solid content with de-ionized water before using, named as EA emulsion.

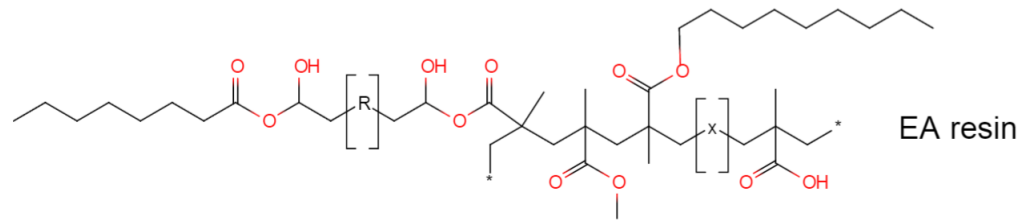

Figure 2. Schematic structure of epoxy-acrylic (EA) resin after two-step esterification process

2.3 Preparation of coating sample

Different kinds of materials were used as coating barrier, as listed in Table 1. The coating procedure was described by using SiO_2-PABC-Gr as an example. 50 mL EA emulsion were taken and mixed with 0.5 g SiO_2-PABC-Gr, dispersed by high speed homogenizer (10000 rmp) for 10 min. Then a certain amount of amino resin was added as curing agent, and further highly dispersed for 5 min. The coating was kept still for c.a. 2 h before coated on low carbon steel. After that, wire rod coater (200 μm) was used to paint the coating on the polished low carbon steel. The paint film was dried at ambient (c.a. 25 °C) for 2 h, and further cured at 150 °C overnight. Then it was kept in ambient for at least 7 days before testing. For simple, EA resin with SiO_2-PABC-Gr as barriers was named as EA resin + SiO_2-PABC-Gr. Others were dominated in the same way.

Table 1. Barrier materials used for different coatings with 50 mL EA emulsion (40 wt.% solid content)

Sample No.	Materials	Weight (g)
0	/	/
1	Graphene	0.005
2	SiO_2	0.5
3	SiO_2-PABC-Gr	0.5
4	SiO_2-PCBC-Gr	0.5

2.4 Measurements

The chemical groups of coatings were characterized by FT-IR using a Perkin-Elmer Spectrum one spectrometer. The XRD patterns were recorded with a Shimadzu (Japan) D/Max-2500 diffractometer using monochromatized, nickel-filtered $Cu_{K\alpha}$ radiation. The morphology of the barriers was observed using SEM (Hitachi S-8000, Japan) in a secondary electron scattering mode at 5 kV. Raman spectra were obtained using a Raman Station (B&WTEK, BWS435-532SY) with a laser operating at 532 nm. The thicknesses of composite coatings were tested by coating thickness gauge (Guangzhou Guoou Electronic Technology Co.). The corrosion rates of coatings were monitored by an electrochemical workstation CHI660E (Shanghai Chenhua Device Co., China). The Potentiodynamic polarization was measured with platinum electrode and calomel electrode and the electrolyte was prepared by 3.5 wt% NaCl solution. The initial voltage was set as -0.8V while the final voltage was set as -0.1V. Meanwhile, the scan rate was used by 0.01V/s and the sensitivity was 10^{-8}. The electrochemical impedance spectroscopes (EIS) were tested while the high frequency was 100000Hz, low frequency was 1Hz, and amplitude was 0.005V.

3. RESULTS AND DISCUSSION

3.1 Structure of different barriers

The IR spectra were recorded for different materials (Figure 3) in order to judge whether or not the composite was formed. For pure SiO_2 particles (Figure 3(a)), only absorption peaks corresponding to OH (3300 cm^{-1}), C=O (1650 cm^{-1}), C-O (1080 cm^{-1}, 936 cm^{-1}), and Si-O-Si (795 cm^{-1}) were observed. Graphene showed very few organic groups (Figure 3(d)), indicating low defects on the sheets (similar results can be referred to Raman spectra in Figure 5). For the SiO_2-PABC-Gr (Figure 3(e)) and SiO_2-PCBC-Gr (Figure 3(f)) composite, besides all the peaks belonging to SiO_2 particles, there were some new peaks emerging or changing. The first is the peak at about 2950 cm^{-1}, which belongs to CH&CH_2. The presence of this peak indicated that both ligands successfully connected to SiO_2 particles and the intensity enhancement of C=O peak at 1650 cm^{-1} also proved the bonding of the ligands. The second is the C-O peak at 1050 cm^{-1}. There was a significant change for sample SiO_2-PABC-Gr, where the broad peak became sharp. As a contrast, almost no variation happed for sample SiO_2-PCBC-Gr in IR spectrum, suggesting no bonding situation changed. The sharp enhancement of C-O peak in SiO_2-PABC-Gr sample perhaps can be attributed to the linking of graphene on the SiO_2 particles. PABC contains COOH and NH_2 groups, which can anchor on SiO_2 and graphene sheets respectively. The surface of SiO_2 surface was alkaline due to the using of NH_4OH in Stöber method [39-40], thus SiO_2 particles can connect with the COOH group of PABC. Meanwhile, the defects and carbon rings of graphene sheets can interact with NH_2 [12, 16, 41], leading to a high dispersion stability. As a contrast, PCBC with two COOH groups can only connect with SiO_2 particles, leaving graphene free. As graphene sheets had no connection with SiO_2, phase separation happened (Figure 1).

The XRD patterns of different barriers were characterized and displayed in Figure 4. The graphene showed a peak at $2\theta=26.0^{o}$ (Figure 4 (a)), which is in agreement with the XRD pattern of

few-layer graphene [42-43]. The peaks at 2θ= 42.8º and 61.9º were caused by MgO [33], which were totally embedded in graphene sheets after combustion reaction and cannot be removed even by acid wash. When SiO_2 particles were concerned, only a large amorphous peak at about 23º appeared (Figure 4 (b)). For the composites, SiO_2-PABC-Gr showed two MgO peaks at 42.8º and 61.9º besides the SiO_2 amorphous peak, whereas SiO_2-PCBC-Gr only exhibited SiO_2 peak. This suggests that the graphene sheets existed in SiO_2-PABC-Gr composites, which were linked by the groups NH_2 of PABC to SiO_2 particles, as indicated before. Meanwhile, PCBC with two COOH groups can only connect with SiO_2 particles, and part of graphene sheets may be removed during centrifugation because of no force between graphene and SiO_2 particles (5000 rmp), resulting in the graphene signal of SiO_2-PCBC-Gr was not as high as that of SiO_2-PABC-Gr.

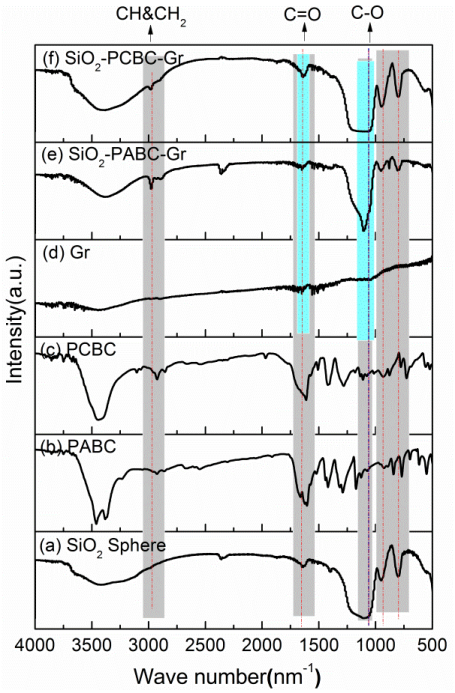

Figure 3. IR spectra of different materials. (a) Silica particles, (b) PABC ligand, (c) PCBC ligand, (d) Graphene (Gr), (e) SiO_2-PABC-Gr and (f) SiO_2-PCBC-Gr

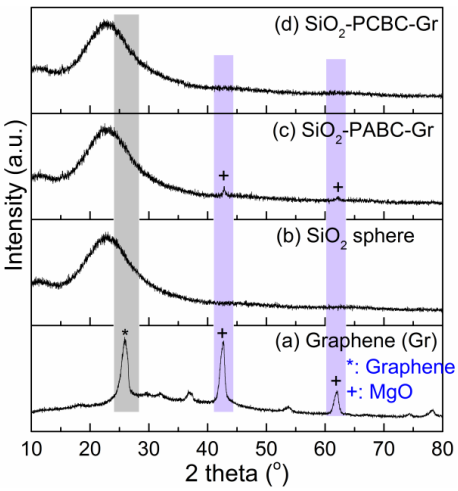

Figure 4. XRD patterns of different materials used as barrier. (a) Graphene (Gr), (b) SiO_2 particles, (c) SiO_2-PABC-Gr and (d) SiO_2-PCBC-Gr

Raman spectroscopy was also used to characterize the synthesized composites. The typical G band (1579 cm^{-1}) and D band (1349 cm^{-1}) of graphene were observed, representing the in-plane bond-stretching motion of the pairs of sp^2 hybridized C atoms (the E_{2g} phonons) and breathing mode of rings or K-point phonons of A_{1g} symmetry, respectively; the second-order D (2D) band at 2695 cm^{-1} is caused by a two phonon double resonance process [44-45]. The relative low intensity of D peak to G peak suggested that the defect concentration in graphene is low; while the relative high intensity of 2D peak to G peak and the position of 2D lower than 2700 cm^{-1} indicated that the graphene sheets were with few layers[33, 44]. SiO_2-PCBC-Gr possessed 2D peak with relatively low intensity when compared with that of SiO_2-PABC-Gr, suggesting graphene was with thicker layers (caused by agglomeration) in SiO_2-PCBC-Gr samples. All these peaks indicated graphene sheets have been successfully composited with SiO_2 particles. Besides, the peak intensities of SiO_2-PABC-Gr were stronger than those of SiO_2-PCBC-Gr, indicating more graphene in the former sample. This is consistent with the XRD results.

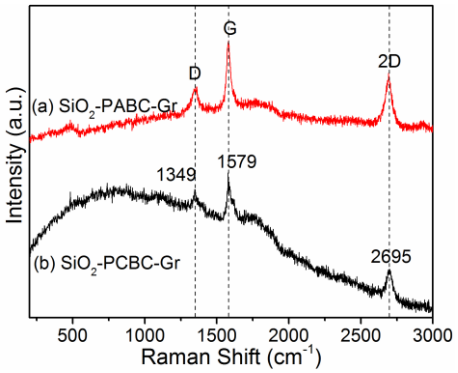

Figure 5. Raman spectra of SiO_2-PABC-Gr (a) and SiO_2-PCBC-Gr (b)

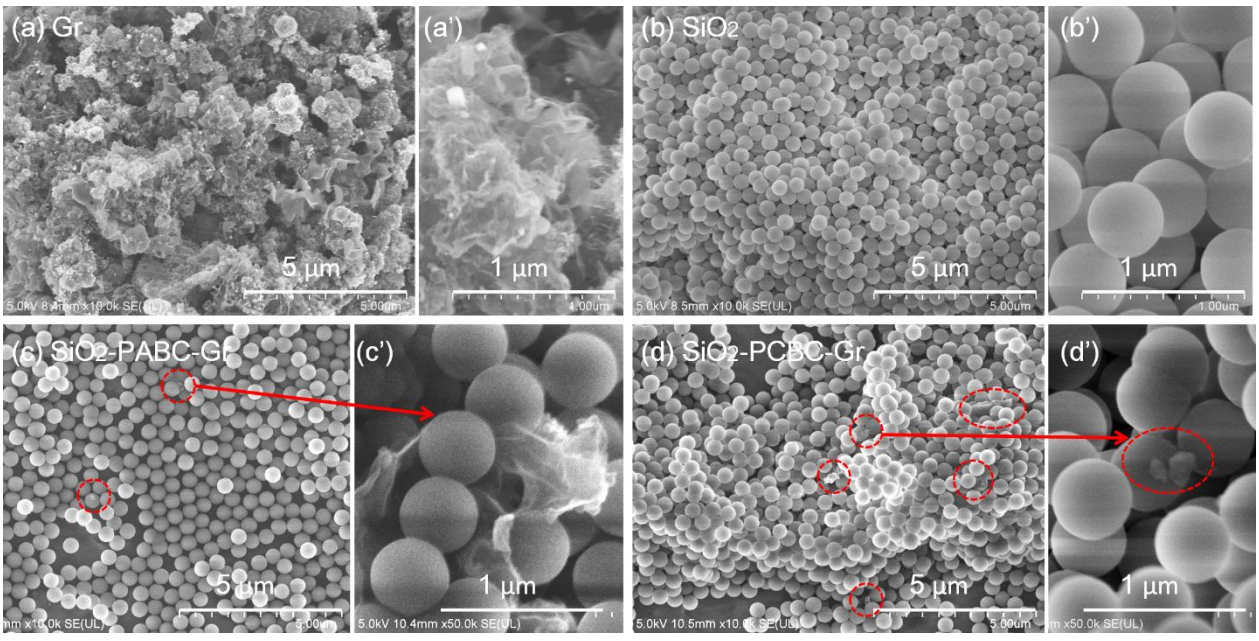

Figure 6. SEM of different materials used as barrier. (a, a') Graphene (Gr), (b, b') SiO_2 particles, (c, c') SiO_2-PABC-Gr, and (d, d') SiO_2-PCBC-Gr

The SEM morphologies of different barriers were shown in Figure 6. The graphene sheets has a porous, almost continuous 3D structure composed of thin corrugated sheets with irregular shapes as shown in Figure 6 (a, a'). The SiO_2 particles displayed a good sphere structure in diameter 450-500 nm (Figure 6 (b, b')). When SiO_2 linked to graphene by PABC, graphene agglomerations can seldom be observed at low magnification (Figure 6 (c)), indicating a homogeneous dispersion of graphene. When the few small agglomerations were observed at high magnification, unfolded graphene thin layers were observed (Figure 6 (c')). As a contrast, the SiO_2-PCBC-Gr samples had more graphene agglomerations (Figure 6 (d)), which were in a crouched structure (Figure 6 (d')). This is consistent with Raman spectra.

3.2 Electrochemical properties of coatings with different barrier

In order to explore the morphologies of coatings with different barriers, the samples were characterized by metallurgical microscope, as shown in Figure 7. As the low carbon steel was covered by a thin layer of tin as corrosion protector, it was burnished to remove the tin layer, resulting in stripe morphology (Figure 7(a)). With the EA coating, the stripe shape was smoothed slightly (Figure 7(b)).

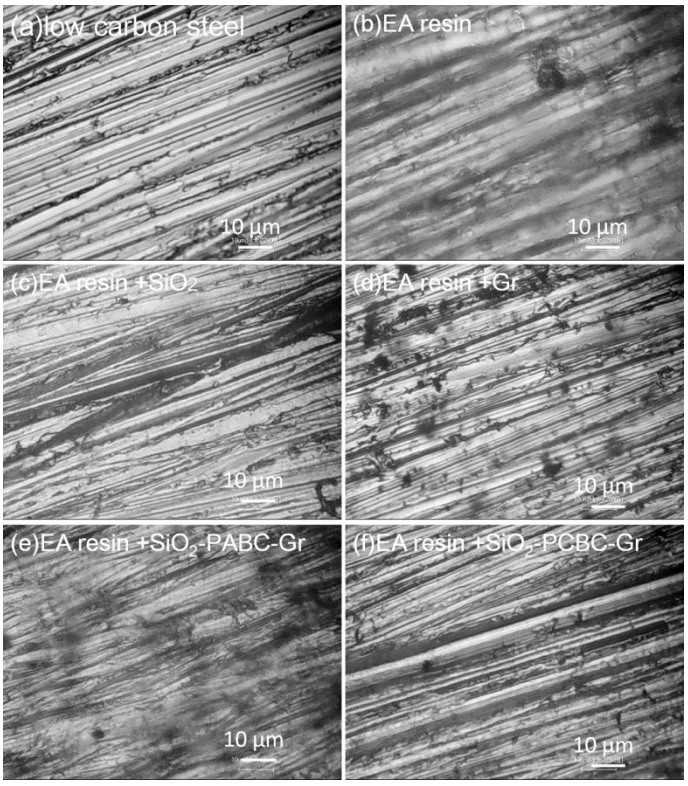

Figure 7. Metallurgical morphologies of pure low carbon steel with different barriers in coatings barriers. (a) No coating, (b) with EA resin, (c) with EA resin +SiO_2 particles, (d) with EA resin +graphene, (e) with EA resin + SiO_2-PABC-Gr and (f) with EA resin + SiO_2-PCBC-Gr

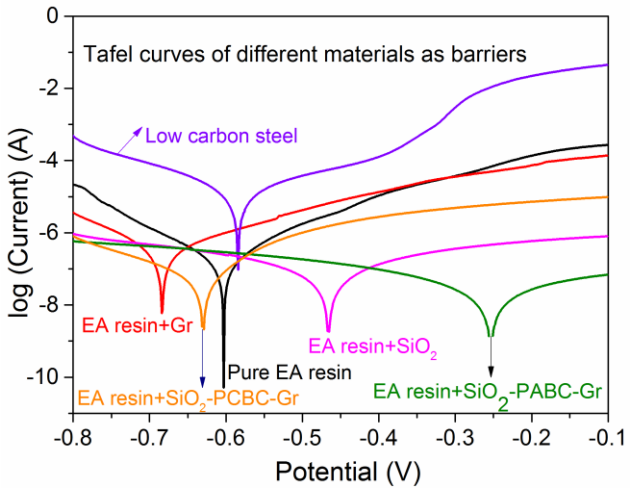

Figure 8. Potentiodynamic polarization curves of pure low carbon steel with different barriers in coatings. (a) Pure low carbon steel, (b) with EA resin, (c) with EA resin +SiO_2 particles, (d) with EA resin +graphene, (e) with EA resin + SiO_2-PABC-Gr and (f) with EA resin + SiO_2-PCBC-Gr

The surface with EA resin+SiO_2 as barrier (Figure 7(c)) became smoother than the previous two samples. But when the barrier changed to EA resin + graphene, many black dots can be obviously seen, which probably caused by the agglomerations of 3D graphene sheets since they are hydrophobic and difficult to be dispersed in water (Figure 7(d)). This poor dispersion of graphene can accelerate the corrosion process, as shown in the following electrochemical test (Figure 8 and Figure 9). When using bifunctional ligand PABC to connect graphene and SiO_2 particles, the smoothness of the surface improved greatly (Figure 7(e)). Conversely, the smoothness of the coating had almost no change when SiO_2-PCBC-SiO_2 was used as barrier and some black points appeared, corresponding to the graphene aggregates (Figure 7(f)).

Figure 8 shows the polarization curves of the coatings with different materials as barrier, and the corresponding parameters are summarized in Table 2 such as corrosion current density (i_{corr}) corrosion rate (μ) and corrosion inhibition efficiency (η). The i_{corr} and corrosion rate μ of EA resin (i_{corr} = 1.65×10^{-7} A cm^{-2}, μ = 0.00172 $g\cdot m^{-2}\cdot h^{-1}$) were lower than the values of EA resin +Gr (i_{corr} = 3.73×10^{-7} A cm^{-2}, μ = 0.00389 $g\cdot m^{-2}\cdot h^{-1}$), but higher than those of EA resin+SiO_2 (i_{corr} = 1.29×10^{-7} A cm^{-2}, μ = 0.00134 $g\cdot m^{-2}\cdot h^{-1}$). It means that EA resin +SiO_2 had better anticorrosion ability, while the composite containing graphene impaired the corrosion resistance. This is consistent with the result of coatings' morphology (Figure 7(d)), which can be attributed to the agglomerations of graphene because of its hydrophobic nature. Furthermore, non-uniform dispersed graphene can even accelerate the corrosion because $O_2/H_2O/Cl^-$ penetrated to the metal substrate more easily though the edges of graphene sheets by forming galvanic corrosion [8, 14, 46]. The coatings with EA+SiO_2-PABC-Gr had the lowest i_{corr} (2.41×10^{-8} A cm^{-2}) and corrosion rate μ (0.00025 $g\cdot m^{-2}\cdot h^{-1}$), the corrosion inhibition efficiency (η) attained to 99.865%; the i_{corr} of SiO_2-PABC-Gr containing coating was about 7 times lower than the value of pure EA resin coating (i_{corr} = 1.65×10^{-7} A cm^{-2}). When using SiO_2-PCBC-Gr as barrier, the corrosion resistance can also be enhanced, but a little bit worse than the coating with SiO_2-PABC-Gr (i_{corr} = 5.97×10^{-8} A cm^{-2}, μ = 0.00062 $g\cdot m^{-2}\cdot h^{-1}$, η = 99.667%). This result verified the

previous results that the PABC ligand can efficiently link graphene to SiO_2 particles, improving its dispersing situation (Figure 1, Figure 3, Figure 6 and Figure 7). The anticorrosion ability of SiO_2-PABC-Gr (i_{corr} = 2.41× 10^{-8} A cm^{-2}) can compare favorably with the values of polypyrrole-intercalated graphene (i_{corr} = 7.73×10^{-9} A cm^{-2}) [19] and the rGO modified ZnAl-LDH (i_{corr} = 7.33× 10^{-8} A cm^{-2}) [6].

Table 2. Electrochemical polarization parameters of different composite coatings after 3 hours of immersion in 3.5wt% NaCl solution (pH=7.0)

Samples	E_{corr} （V）	i_{corr} (A cm^{-2})	*ba*	*-bc*	μ (g·m^{-2}·h^{-1})	η (%)
low carbon steel	-0.584	1.77×10^{-5}	5.158	6.806	0.18478	-
EA resin	-0.603	1.65×10^{-7}	11.07	10.13	0.00172	99.072%
EA resin+SiO_2 particles	-0.487	1.29×10^{-7}	5.667	4.355	0.00134	99.273%
EA resin+Gr	-0.684	3.73×10^{-7}	6.306	9.022	0.00389	97.897%
EA resin+SiO_2-PABC-Gr	-0.254	2.41×10^{-8}	4.248	5.447	0.00025	99.865%
EA resin+SiO_2-PCBC-Gr	-0.630	5.97×10^{-8}	11.151	6.693	0.00062	99.667%
M-rGO-ZnAl-LDH (2:1–0.5 wt%) [6]	-0.635	7.33×10^{-8}	12.02	8.686	0.0007	99.69%
PPy-G0.5%[19]	-0.596	7.73×10^{-9}	4.438	6.674	-	99.99%
Epoxy/0.5 f-GQDs[13]	-0.574	2.28×10^{-6}	7.353	5.155	-	92.2%

E_{corr} : Corrosion potential; *-bc*: Cathode polarization slope;
i_{corr} : corrosion current density; μ **:** corrosion rate;
ba :Anodic polarization slope; η : corrosion inhibition efficiency.

In order to have a comprehensive detection of corrosion resistance, electrochemical impedance spectroscopes (EIS) were tested, and the parameters influencing the corrosion resistances can be monitored, such as capacitance of coating, the resistance of micro-pores and the resistance of substrates' corrosion and so on. The Nyquist plots were shown in Figure 9. In Figure 9, the diameter of semicircles increased in the following sequence: low carbon steel ＜ EA resin + graphene ＜ EA resin ＜ EA resin + SiO_2-PCBC-Gr＜ EA resin + SiO_2＜ EA resin + SiO_2-PABC-Gr. It can roughly suggest that the coatings with EA resin +SiO_2-PABC-Gr barrier has a higher resistance than those with a single component as a barrier. The corresponding equivalent circuit diagram was shown in Figure 10 and the EIS fitting parameters were summarized in Table 3, where Rs was on behalf of electrolyte resistance, Rc was coating resistance, Rct was charge transfer resistance, CPE_c was coating capacitance, and CPE_{dl} was double layer capacitance. Normally, high Rc value represented the good anticorrosion performance of the coating [47]. The Rc of EA resin + SiO_2-PABC-Gr was 3.93×10^5 Ω cm^{-2}, which is about 12 times larger than the value of EA resin+SiO_2-PCBC-Gr (3.24×10^4 Ω cm^{-2}) and . The lower resistances of graphene and SiO_2-PCBC-Gr containing coating were caused by the agglomeration of graphene sheets, and inhomogeneous dispersed graphene accelerated the corrosion, as reported before [8, 14, 46]. The application of PABC can anchor graphene to SiO_2 particles, improving its dispersion in EA waterborne resin. Thus, the pinholes can be blocked efficiently and the anticorrosion ability (resistance) can be improved.

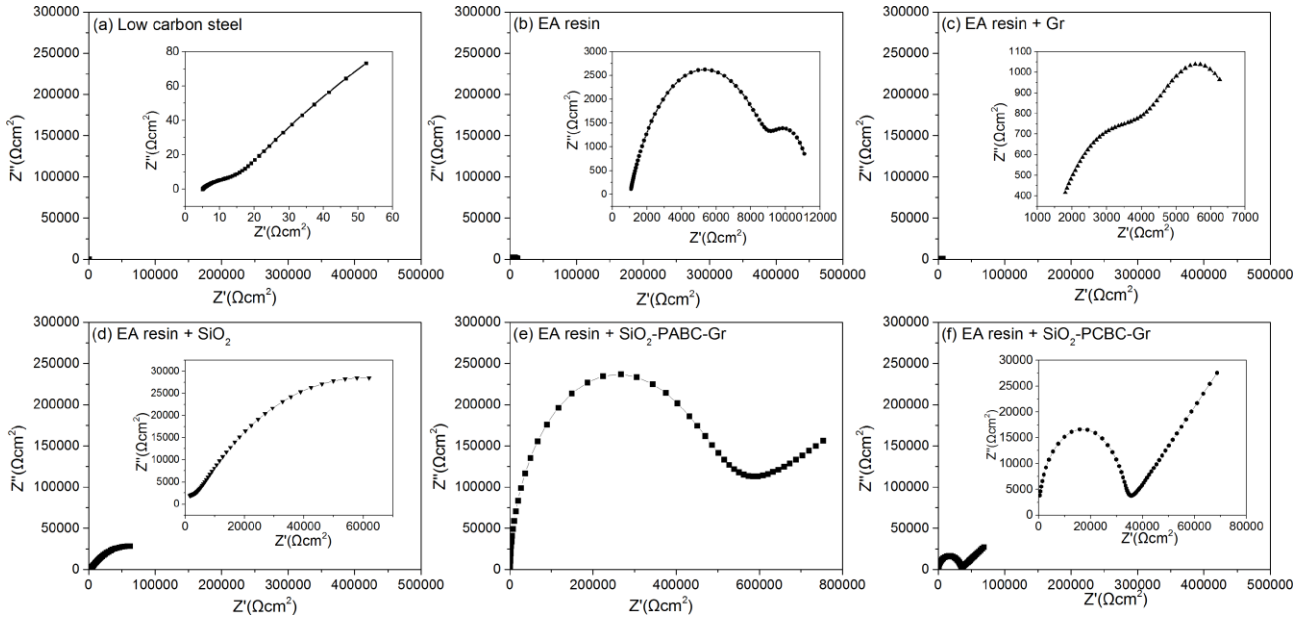

Figure 9. EIS measurements of pure low carbon steel with different barriers in coatings. (a) Pure low carbon steel, (b) EA resin, (c) EA resin+ Gr, (d) EA resin+ SiO_2, (e) EA resin + SiO_2-PABC-Gr, (f) EA resin + SiO_2-PCBC-Gr

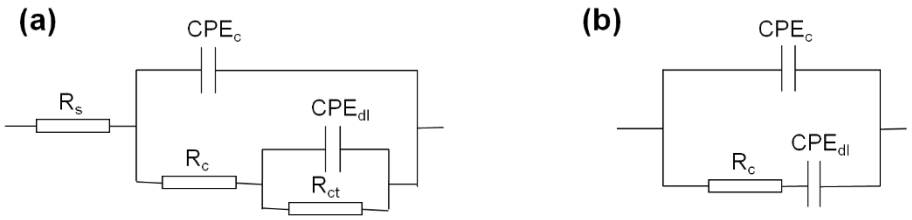

Figure 10. Equivalent circuit used to fit the measured impedance data. (a) is suitable for pure low carbon steel, EA resin, EA resin+ Gr,. (b) is suitable for EA resin+ SiO_2, EA resin + SiO_2-PABC-Gr and EA resin + SiO_2- PCBC-Gr

The Bode plots were show in Figure 11. The impedance in low frequency region indicates the capacity of coating shield to corrosion medium. In this region, the impedance changed as follows: low carbon steel ＜ EA resin ＜ EA resin+ Gr ＜ EA resin + SiO_2 ＜ EA resin + SiO_2-PCBC-Gr ＜ EA resin + SiO_2-PABC-Gr. The Bode plot of EA resin + SiO_2-PABC-Gr is much higher than that of EA resin + SiO_2-PCBC-Gr, indicating that the coating containing EA resin + SiO_2-PABC-Gr as barrier had a brilliant anti-corrosion ability.

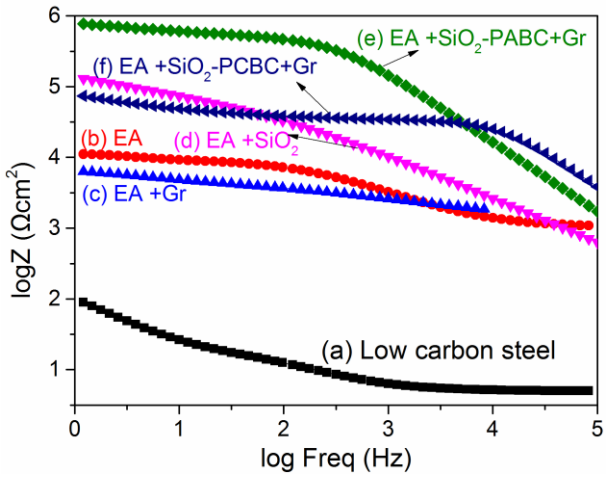

Figure 11. Bode plots of pure low carbon steel with different barriers in coatings. (a) Pure low carbon steel, (b) EA resin, (c) EA resin+ Gr, (d) EA resin+ SiO_2, (e) EA resin + SiO_2-PABC-Gr, (f) EA resin + SiO_2-PCBC-Gr

Table 3 Summary of EIS fitting parameters for different samples

Samples	R_s (Ω/cm^2)	R_c (Ω/cm^2)	n_1	CPE_c (F/cm^2)	R_{ct} (Ω/cm^2)	n_2	Q_{ct} (F/cm^2)	Y_1	Y_2
low carbon steel	4.98×10^{0}	1.59×10^{1}	7.47×10^{-1}	1.33×10^{-4}	-	-	-	6.31×10^{-4}	-
EA resin	1.02×10^{3}	8.56×10^{3}	7.00×10^{-1}	8.44×10^{-8}	1.91×10^{3}	9.93×10^{-1}	2.40×10^{-5}	7.40×10^{-7}	2.46×10^{-5}
EA resin+SiO_2 sphere	-	5.65×10^{4}	6.27×10^{-1}	3.65×10^{-7}	-	-	3.13×10^{-1}	5.41×10^{-6}	-
EA resin+Gr	1.07×10^{3}	4.23×10^{3}	4.04×10^{-1}	1.54×10^{-7}	2.56×10^{3}	6.82×10^{-1}	2.03×10^{-5}	1.22×10^{-5}	5.19×10^{-5}
EA resin+SiO_2-PABC-Gr	-	3.93×10^{5}	9.80×10^{-1}	1.21×10^{-4}	-	-	2.53×10^{-1}	1.52×10^{-6}	-
EA resin+SiO_2-PCBC-Gr	-	3.24×10^{4}	1.00×10^{0}	4.09×10^{-10}	-	-	4.14×10^{-1}	9.49×10^{-6}	-

Based on the previous structure characterization and electrochemical results, a structure sketch was proposed to explain the different performance of SiO_2-PABC-Gr and SiO_2-PCBC-Gr barrier (Figure 12). When using PABC as coupling agent, graphene linked to SiO2 through PABC, resulting in high dispersion of graphene sheet (Figure 12 (a)). In this case, more pinholes of the coating can be blocked by highly dispersed graphene, and the anticorrosion resistance improved. As a contrast, PCBC ligand, containing two COOH group, can only connect two SiO_2 particles, and the agglomeration of graphene happened (Figure 12 (b)). Thus more pinholes were opened to the low carbon steel, and

$O_2/H_2O/Cl^-$ can reach to the substrate, causing larger corrosion current density.

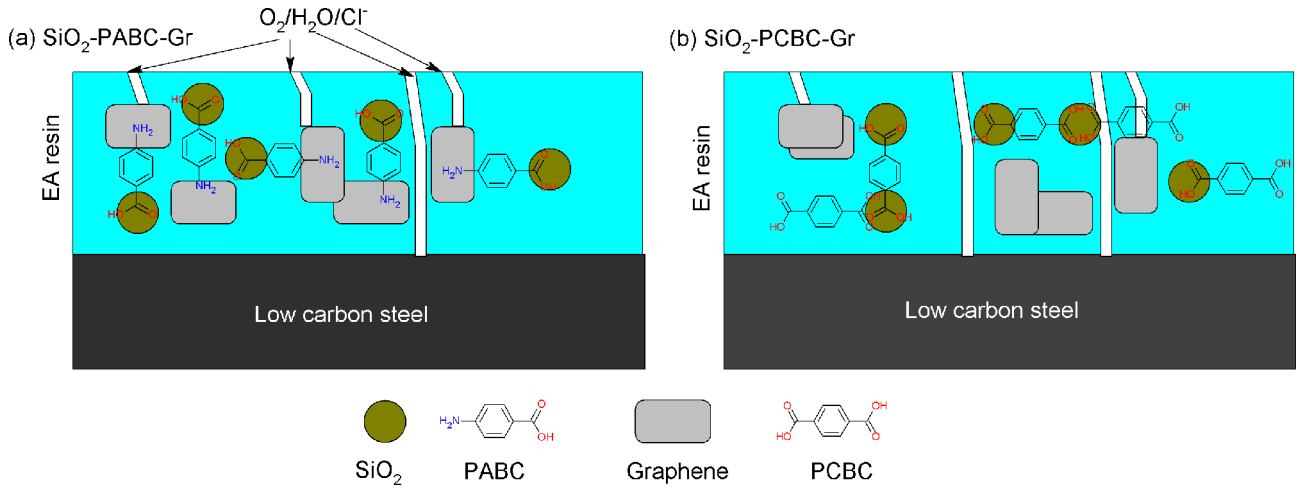

Figure 12. Sketch of different barriers in EA resins

4. CONCLUSION

A novel graphene barrier was designed by using a bifunctional ligand *p*-aminobenzoic acid (PABC) to connect SiO_2 particles and graphene (SiO_2-PABC-Gr). The COOH and NH_2 groups of PABC can link to SiO_2 and graphene, respectively. This approach can improve the dispersion of graphene in both the composite powder and coating. As a comparison, the aggregation of graphene cannot be efficiently avoided by using *p*-phthalic acid as the linker of SiO_2 particles and graphene (SiO_2-PCBC-Gr), while the two COOH groups in a *p*-phthalic acid molecular can only interact with SiO_2 particles. The EA resin was used as the binder of the coating, which contained COOH groups to connect with SiO_2 particles. When used as anticorrosion protection coating of low carbon steel, the corrosion current density i_{corr} and corrosion rate μ can be greatly improved significantly by SiO_2-PABC-Gr barrier. The i_{corr} of SiO_2-PABC-Gr containing coating was only 2.41×10^{-8} A cm^{-2}, about 20 times lower than the value of pure EA resin coating (i_{corr} = 1.65×10^{-7} A cm^{-2}); and the corrosion inhibition efficiency η can even reach to 99.865%.

ACKNOWLEDGEMENT
This research was supported by National Natural Science Foundation of China (grant number 21601121); College Student Research Training Program of SUES (grant number cx1704009); and the Program for Professor of Special Appointment (Eastern Scholar) at Shanghai Institutions of Higher Learning (grant number QD2016037).

References

1. M. Bandiera, R. Balk and M.J. Barandiaran, *Eur. Polym. J.*, 97 (2017) 77.
2. P. Berce, S. Skale, T. Razborsek and M. Slemnik, *J. Appl. Polym. Sci.*, 134 (2017) doi: 10.1002/app.45142.
3. X. Yin, C. Dong and Y. Luo, *Colloid Polym. Sci.*, 295 (2017) 2423.

4. H. Zhou, H. Wang, H. Niu, Y. Zhao, Z. Xu and T. Lin, *Adv. Funct. Mater.*, 27 (2017) doi: 10.1002/adfm.201604261.
5. M. Liu, X. Mao, H. Zhu, A. Lin and D. Wang, *Corros. Sci.*, 75 (2013) 106.
6. D. Yu, S. Wen, J. Yang, J. Wang, Y. Chen, J. Luo and Y. Wu, *Surf. Coat. Technol.*, 326 (2017) 207.
7. A. Ambrosi and M. Pumera, *Chem. - Eur. J.*, 21 (2015) 7896.
8. A.U. Chaudhry, V. Mittal and B. Mishra, *RSC Adv.*, 5 (2015) 80365.
9. A. Kumar, R. Anant, K. Kumar, S.S. Chauhan, S. Kumar and R. Kumar, *RSC Adv.*, 6 (2016) 113405.
10. X. Zheng, X. Xiong, J. Yang, D. Chen, R. Jian and L. Lin, *Chem. Eng. J.* , 333 (2018) 153.
11. Y. Zhang, P. Yu, J. Wang, Y. Li, F. Chen, K. Wei and Y. Zuo, *Appl. Surf. Sci.*, 433 (2018) 927.
12. B. Ramezanzadeh, G. Bahlakeh, M.H. Mohamadzadeh Moghadam and R. Miraftab, *Chem. Eng. J.* , 335 (2018) 737.
13. S. Pourhashem, E. Ghasemy, A. Rashidi and M.R. Vaezi, *J. Alloys Compd.*, 731 (2018) 1112.
14. J. Lee and D. Berman, *Carbon*, 126 (2018) 225.
15. J. Ding, O. ur Rahman, W. Peng, H. Dou and H. Yu, *Appl. Surf. Sci.*, 427 (2018) 981.
16. M. Cui, S. Ren, H. Zhao, Q. Xue and L. Wang, *Chem. Eng. J.* , 335 (2018) 255.
17. M. Wang, M. Tang, S. Chen, H. Ci, K. Wang, L. Shi, L. Lin, H. Ren, J. Shan, P. Gao, Z. Liu and H. Peng, *Adv. Mater.* , 29 (2017) doi: 10.1002/adma.201703882.
18. M.A. Raza, A. Ali, F.A. Ghauri, A. Aslam, K. Yaqoob, A. Wasay and M. Raffi, *Surf. Coat. Technol.*, 332 (2017) 112.
19. S. Qiu, W. Li, W. Zheng, H. Zhao and L. Wang, *ACS Appl. Mater. Interfaces*, 9 (2017) 34294.
20. C.-Y. Ho, S.-M. Huang, S.-T. Lee and Y.-J. Chang, *Appl. Surf. Sci.*, (2017) doi: 10.1016/j.apsusc.2017.10.129.
21. H. Hayatdavoudi and M. Rahsepar, *J. Alloys Compd.*, 727 (2017) 1148.
22. E. Ghiamati Yazdi, Z.S. Ghahfarokhi and M. Bagherzadeh, *New J. Chem.*, 41 (2017) 12470.
23. M. Ganjaee Sari, M. Shamshiri and B. Ramezanzadeh, *Corros. Sci.*, 129 (2017) 38.
24. M. Cui, S. Ren, S. Qin, Q. Xue, H. Zhao and L. Wang, *Corros. Sci.*, 131 (2018) 187.
25. K.S. Novoselov, A.K. Geim, S.V. Morozov, D. Jiang, Y. Zhang, S.V. Dubonos, I.V. Grigorieva and A.A. Firsov, *Science*, 306 (2004) 666.
26. S. Balasubramanyan, S. Sasidharan, R. Poovathinthodiyil, R.M. Ramakrishnan and B.N. Narayanan, *New J. Chem.*, 41 (2017) 11969.
27. C. Cui, J. Huang, J. Huang and G. Chen, *Electrochim. Acta*, 258 (2017) 793.
28. X. Yu, H. Cheng, M. Zhang, Y. Zhao, L. Qu and G. Shi, *Nat. Rev. Mater.*, 2 (2017) 17046.
29. Y. Hernandez, V. Nicolosi, M. Lotya, F.M. Blighe, Z. Sun, S. De, I.T. McGovern, B. Holland, M. Byrne, Y.K. Gun'Ko, J.J. Boland, P. Niraj, G. Duesberg, S. Krishnamurthy, R. Goodhue, J. Hutchison, V. Scardaci, A.C. Ferrari and J.N. Coleman, *Nat. Nanotechnol.*, 3 (2008) 563.
30. T. Ohta, A. Bostwick, T. Seyller, K. Horn and E. Rotenberg, *Science*, 313 (2006) 951.
31. C. Virojanadara, M. Syvajarvi, R. Yakimova, L.I. Johansson, A.A. Zakharov and T. Balasubramanian, *Phys. Rev. B: Condens. Matter Mater. Phys.*, 78 (2008) 245403/1.
32. X. Li, W. Cai, L. Colombo and R.S. Ruoff, *Nano Lett.*, 9 (2009) 4268.
33. L. Wang, B. Wei, P. Dong, Q. Miao, Z. Liu, F. Xu, J. Wu, J. Lou, R. Vajtai and W. Fei, *Mater. Des.*, 92 (2016) 462.
34. J.L. Sabourin, D.M. Dabbs, R.A. Yetter, F.L. Dryer and I.A. Aksay, *ACS Nano*, 3 (2009) 3945.
35. M. Zhou, A. Zhang, Z. Dai, Y.P. Feng and C. Zhang, *J. Phys. Chem. C*, 114 (2010) 16541.
36. N.-Q. Deng, H. Tian, Z.-Y. Ju, H.-M. Zhao, C. Li, M.A. Mohammad, L.-Q. Tao, Y. Pang, X.-F. Wang, T.-Y. Zhang, Y. Yang and T.-L. Ren, *Carbon*, 109 (2016) 173.
37. M. Humood, S. Qin, Y. Song, K. Polychronopoulou, Y. Zhang, J.C. Grunlan and A.A. Polycarpou, *ACS Appl. Mater. Interfaces*, 9 (2017) 1107.
38. P. Zhu, J. Zang, J. Zhu, Y. Lu, C. Chen, M. Jiang, C. Yan, M. Dirican, R.K. Selvan, D. Kim and X. Zhang, *Carbon*, 126 (2018) 594.

39. W. Stoeber, A. Fink and E. Bohn, *J. Colloid Interface Sci.*, 26 (1968) 62.
40. X.-D. Wang, Z.-X. Shen, T. Sang, X.-B. Cheng, M.-F. Li, L.-Y. Chen and Z.-S. Wang, *Journal of Colloid and Interface Science*, 341 (2010) 23.
41. M. Park, K. Song, T. Lee, J. Cha, I. Lyo and B.-S. Kim, *ACS Appl. Mater. Interfaces*, 8 (2016) 21595.
42. J. Zhao, Y. Guo, Z. Li, Q. Guo, J. Shi, L. Wang and J. Fan, *Carbon*, 50 (2012) 4939.
43. A. Chakrabarti, J. Lu, J.C. Skrabutenas, T. Xu, Z. Xiao, J.A. Maguire and N.S. Hosmane, *J. Mater. Chem.*, 21 (2011) 9491.
44. A.C. Ferrari, J.C. Meyer, V. Scardaci, C. Casiraghi, M. Lazzeri, F. Mauri, S. Piscanec, D. Jiang, K.S. Novoselov, S. Roth and A.K. Geim, *Phys. Rev. Lett.*, 97 (2006) 187401/1.
45. C. Zhu, S. Guo, Y. Fang and S. Dong, *ACS Nano*, 4 (2010) 2429.
46. M. Schriver, W. Regan, W.J. Gannett, A.M. Zaniewski, M.F. Crommie and A. Zettl, *ACS Nano*, 7 (2013) 5763.
47. L. Shen, Y. Zhao, Y. Wang, R. Song, Q. Yao, S. Chen and Y. Chai, *J. Mater. Chem. A*, 4 (2016) 5044.